Computers and Mathematics with Applications 59 (2010) 2315–2325

Contents lists available at ScienceDirect

Computers and Mathematics with Applications

journal homepage: www.elsevier.com/locate/camwa

Application of the Lattice-Boltzmann method to the modeling of population blob dynamics in 2D porous domains

A.G. Yiotis [a,*], M.E. Kainourgiakis [a], E.S. Kikkinides [b], A.K. Stubos [a]

[a] National Center for Scientific Research "Demokritos", 15310 Athens, Greece

[b] Department of Mechanical Engineering, University of Western Macedonia, Bakola and Sialvera street, 50100 Kozani, Greece

ARTICLE INFO

Keywords:
Lattice Boltzmann
Two-phase flow
Blobs
Porous media

ABSTRACT

In the present paper, the Lattice-Boltzmann method is employed for the simulation of immiscible two-phase flow through a 2D porous domain when the volume fraction of the non-wetting phase is relatively low and thus it flows in the form of disconnected blobs. The flow problem is solved using an immiscible two-phase LB model where interfacial forces are expressed in terms of the chemical potential through the Gibbs–Duhem equation. We study the population dynamics of the non-wetting fluid blobs, namely the temporal evolution of the average blob size, with respect to the applied body force and the wetting phase volume fraction. Our results show that the system reaches a "steady state" where the average values of the studied parameters, such as the superficial velocities of both phases, and the number and size distribution of the blobs remain practically constant in time, although the temporal fluctuations around average values may be significant. We show that the average volume of the blobs decreases (and the population of the blobs increases) as the body force increases, namely as the viscous forces become dominant over capillary forces. The effect of the wetting volume fraction on the number of the blobs is more complex; as the wetting volume fraction decreases at constant body force, the blobs cover larger areas within the pore space producing larger pressure gradients and the dynamic breakup of blobs intensifies resulting in increasing blob numbers. However, below a critical value of the wetting volume fraction, the number of blobs begins to decrease and the non-wetting phase begins to span the entire pore network.

© 2010 Elsevier Ltd. All rights reserved.

1. Introduction

Two-phase flow in porous media is encountered in a plethora of energy-related, environmental-related and other industrial applications such as oil/gas recovery, soil remediation and geothermal processes. The two phases can be either a gas and a liquid phase or two immiscible and/or partial miscible liquid phases. Typical examples of the two phases being gas and liquid are the case of solution gas during primary production of light oil, and the case of the flowing gas phase dispersed in the form of bubbles during the aggressive production of heavy oil from unconsolidated sands ("foamy" oil). A typical example of the two phases being immiscible liquids is the presence of NAPL (Non-Aqueous Phase Liquid) pollutants in an aquifer. Depending on the relative amount of the two phases in the porous medium, the phases can be both continuous or one phase can be discontinuous and randomly distributed inside the other phase. The case of a discontinuous, immiscible and randomly distributed non-wetting fluid into a porous medium has attracted significant attention, since it is encountered in a number of practical applications, and is the focus of the present study.

* Corresponding author. Tel.: +30 210 6503403.
E-mail addresses: yiotis@ipta.demokritos.gr (A.G. Yiotis), kainourg@ipta.demokritos.gr (M.E. Kainourgiakis), kikki@uowm.gr (E.S. Kikkinides), stubos@ipta.demokritos.gr (A.K. Stubos).

0898-1221/$ – see front matter © 2010 Elsevier Ltd. All rights reserved.
doi:10.1016/j.camwa.2010.01.023

The discontinuous non-wetting fluid (nw-phase) flows within the pore void in the form of blobs (otherwise called ganglia) [1–3], while the wetting fluid (w-phase) forms a continuous spanning film that covers the pore walls. The randomness and heterogeneity of the porous medium can result in the production of a distribution of blobs of different sizes and shapes. The blobs flow through the porous medium under the combined effect of capillary, viscous and buoyancy forces. The relative magnitude of these forces determines the rate at which two or more blobs coalesce to form a larger one and the rate at which single blobs breakup into smaller ones. These forces also determine the ratio of the mobile blobs that flow through the pore space to the stranded blobs that are immobilized in low permeability regions of the porous medium. The mobilization of stranded blobs is of key importance to several processes such Enhanced Oil Recovery (EOR) and soil remediation and can be realized by injecting a wetting fluid, i.e. water, into the porous block or by reducing the surface tension of the fluid/fluid interface, thus reducing the capillary forces restraining the ganglia. In general, all blobs, both mobile and stranded, undergo a continuous "life-circle" during which they continuously breakup into smaller blobs and coalesce with other to form larger ones. However, given any random initial phase distribution and allowing for a sufficiently large amount of time, the system reaches a "steady state" where the average values of the flow parameters, such as the superficial velocities of the w-phase and the nw-phase, the number of blobs, and the mobile to stranded blob ratio remain practically constant in time, although the temporal fluctuations around average values may be significant.

The problem is mainly characterized by the Capillary number $Ca = \mu_w u_w/\gamma$, which expresses the ratio of viscous forces over interfacial forces at fluid/fluid interfaces. u_w is the superficial velocity of the wetting fluid, μ_w is viscosity of the wetting fluid and γ is the interfacial tension at the fluid/fluid interface. Other parameters that determine the physics of the flow problem include the phase fraction of the wetting fluid S_w, the density ratio $D = \rho_{nw}/\rho_w$, the viscosity ratio $M = \mu_{nw}/\mu_w$, the dynamic contact angle and several parameters that are determined by the geometry of the porous material, such as the porosity ε and the connectivity of the pores (see Refs. [1–6] for more details on the effects of these parameters). In this contribution, we focus on the effects of the Capillary number (through the applied body force G) and the phase fraction on the flow problem.

Several methods have been proposed to model blobs dynamics in porous media, including pore network modeling [1–4], stochastic simulation [5], mechanistic modeling [6] and the recently developed method of Darcian dynamics [7]. The characteristic of such methods is that they rely on simplified transport equations and/or mechanistic rules to determine the spatial distribution and temporal evolution of interfaces. The pressure field is calculated by solving simple flow models, such as Poiseuille or Darcy flow, through simplified void topologies such as pore networks or continuous permeability mediums, while capillary forces at pores are calculated through Laplace's law. These approximations, although crude, have provided the means to qualitatively model population blobs dynamics using reasonable computational resources. On the other hand, the application of such models is limited to simplified pore geometries and their accuracy is limited given that the flow and interfacial physics involved are coupled in macroscopic parameters such as relative permeabilities or coalescence probabilities [4,7].

In recent years, the rapid increase in computational power in conjunction with the continuous development of rigorous Lattice-Boltzmann (LB) models have provided the tools for a more in-depth understanding of the underlying physics of immiscible two-phase flows in porous materials. The LB method is especially useful for complex systems in which the macroscopic governing equations cannot be determined in a straightforward manner while the microscopic physics is adequately described to a certain level of approximation [8]. Several approaches exist for modeling multiphase flows using the LB method. These approaches can be classified in three major groups. One approach is based on the implementation of a pairwise interparticle potential [9,10] between nearest-neighbor molecules of different fluids and a particle distribution function to describe the flow of each fluid. This approach can be easily extended to multiphase, multicomponent systems with any number of components both miscible and immiscible. However, this approach leads to thermodynamic inconsistencies in dense fluids [11] since the intermolecular potential cannot be accurately described by the nearest-neighbor interaction scheme which completely ignores the repulsive core of the Lennard-Jones potential. The second approach utilizes the basic assumptions of the van der Waals (vdW) theory and is based on a free energy formulation of fluid interactions [12]. The basic idea behind this approach is to impose an additional constraint on the equilibrium distribution function so that its second moment reproduces the desired pressure tensor, and hence this approach is often called the pressure method. The third approach is guided by an atomistic formalism where interparticle interactions are introduced by the direct introduction of a forcing term in the LB equation. The forcing term was originally described by He et al. [13] by considering interparticle interaction using a mean-field treatment. Later, He and Doolen [11] improved the above model starting from the BBGKY equations and established the thermodynamic foundations of the LB multiphase models by showing that a kinetic equation that combines Enskog's theory for dense fluids and the mean-field theory for long-range molecular interaction can consistently describe non-ideal gases and dense fluid flows. The equation of state is obtained and the required thermodynamic consistency is achieved. In all cases the basic features of the vdW theory are retained and these set the thermodynamic limits of the validity of these models.

In this work, we examine the dynamics of nw-phase blobs in 2D pore networks using the Lattice-Boltzmann (LB) model proposed by He et al. [14] with an improved numerical scheme which incorporates the Gibbs–Duhem equation as described in [15]. This approach provides the means for a deterministic study of the blob population dynamics in porous media, namely the temporal evolution of the average blob size and the fraction of the immobile blobs with respect to the applied body force and the w-phase volume fraction without the need for mechanistic assumptions or stochastic approaches.

2. Lattice-Boltzmann approach

The LB method is a numerical scheme for the solution of fluid mechanical problems, especially in systems where the fluid–solid interface is very complex [8]. Space, time and momentum are discretized and the fluid behavior is described by the evolution of the single-particle distribution functions. In the present study, the simulation of two-phase flow is based on the method proposed by He et al. [14] implemented as described by Kikkinides et al. [15]. According to this method eighteen space–time functions $f_i(\vec{x}, t)$ and $g_i(\vec{x}, t)$, where $i = 0, 1, 2, \ldots, 8$, are required to describe the system in two dimensions.

Denoting δx the lattice spacing and δt the time step, the microscopic velocity in two dimensions, $\vec{e}$, is discretized in nine vectors (including the null vector), defined as follows:

$$\vec{e}_i = \begin{cases} (0,0)c & i = 0 \\ (\pm 1, 0)c & i = 1, 2 \\ (0, \pm 1)c & i = 3, 4 \\ (\pm 1, \pm 1)c & i = 5, 6, 7, 8 \end{cases} \tag{1}$$

where $c = \delta x/\delta t$.

The spatio-temporal evolution of $f_i(\vec{x}, t)$ and $g_i(\vec{x}, t)$ is assumed to follow the equations:

$$f_i(\vec{x} + \vec{e}_i\delta t, t + \delta t) - f_i(\vec{x}, t) = -\frac{f_i(\vec{x}, t) - f_i^{(eq)}(\vec{x}, t)}{\tau} + \Omega_f \tag{2}$$

and

$$g_i(\vec{x} + \vec{e}_i\delta t, t + \delta t) - g_i(\vec{x}, t) = -\frac{g_i(\vec{x}, t) - g_i^{(eq)}(\vec{x}, t)}{\tau} + \Omega_g \tag{3}$$

where $f_i^{(eq)}$ and $g_i^{(eq)}$ are the equilibrium distribution functions, Ω_f and Ω_g are terms associated with the perturbation of the distribution functions from equilibrium and τ is the relaxation time which is related with the kinematic viscosity ν by:

$$\nu = (\tau - 0.5)RT\delta t. \tag{4}$$

Here, R is the gas constant and T is the absolute temperature. Assuming molar mass equal to unity and recalling that for the ideal gas the equation of state is $p = \rho c_s^2$, where c_s is the speed of sound, and $c_s = c/\sqrt{3}$ [8], the product RT in lattice units can be expressed by $RT = c^2/3$.

Before proceeding, it is convenient to introduce the distribution function, $\Gamma_i(\vec{u})$ derived from the Maxwell–Boltzmann distribution by a Taylor expansion in terms of the Mach number, $\vec{u}/c_s$:

$$\Gamma_i(\vec{u}) = w_i\left[1 + \frac{\vec{e}_i \cdot \vec{u}}{c_s^2} + \frac{(\vec{e}_i \cdot \vec{u})^2}{2c_s^4} - \frac{\vec{u} \cdot \vec{u}}{2c_s^2}\right] \tag{5}$$

where $\vec{u}$ is the fluid velocity and w_i is the appropriate integral weights, with values:

$$w_i = \begin{cases} 4/9 & i = 0 \\ 1/9 & i = 1, 2, 3, 4 \\ 1/36 & i = 5, 6, 7, 8. \end{cases} \tag{6}$$

The equilibrium distribution functions of Eqs. (2) and (3) are associated with Γ_i by the relations:

$$f_i^{(eq)} = \rho\Gamma_i \tag{7}$$

and

$$g_i^{(eq)} = w_i p + \rho RT(\Gamma_i - w_i) \tag{8}$$

where ρ is the density and p is the pressure. The intensive parameters ρ, p and T are related through the van der Waals equation of state:

$$p = \frac{\rho RT}{1 - b\rho} - a\rho^2 \tag{9}$$

where $a = \frac{9}{8}RT/T_r$, $b = 1/3$, $T_r = T/T_c$ and T_c is the critical temperature.

The source term Ω_g which appears in Eq. (3) incorporates the body force density, $\vec{G}$, acting on the fluid, as well as the force $\vec{F}_s$, relevant to the surface tension. Specifically:

$$\Omega_g = -\frac{(2\tau - 1)}{2\tau}(\vec{e}_i - \vec{u}) \cdot [\Gamma_i(\vec{u})(\vec{F}_s + \vec{G}) - (\Gamma_i(\vec{u}) - \Gamma_i(\vec{0}))\vec{\nabla}\psi(\rho)]\delta t \tag{10}$$

where $\psi(\rho)$ is the deviation of the pressure from that corresponding to the ideal gas:

$$\psi(\rho) = p - \rho RT. \tag{11}$$

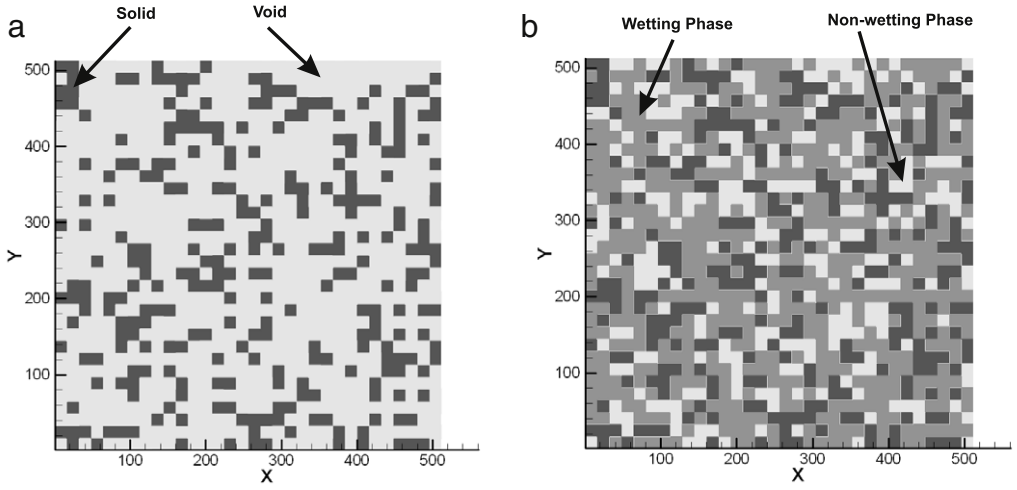

Fig. 1. Schematic of the 2D pore network.

For a van der Waals fluid consisting of particles with collision diameter σ, the force density due to surface tension can be expressed by:

$$\vec{F}_s = a\sigma^2\rho\vec{\nabla}\nabla^2\rho. \tag{12}$$

Finally, the term Ω_f which is responsible for phase separation is calculated by:

$$\Omega_f = -\frac{(2\tau-1)}{2\tau}\frac{(\vec{e}_i-\vec{u})\cdot\vec{F}}{RT}\Gamma_i(\vec{u})\delta t \tag{13}$$

where

$$\vec{F} = -\rho\vec{\nabla}\left(\frac{RT\ln\rho}{1-b\rho}+\frac{RT}{1-b\rho}-2a\rho\right)+\rho RT\vec{\nabla}\ln\rho. \tag{14}$$

The density, velocity and pressure fields are evaluated from the distribution functions $f_i(\vec{x},t)$ and $g_i(\vec{x},t)$ as follows:

$$\rho(\vec{x},t) = \sum_{i=0}^{8} f_i(\vec{x},t) \tag{15}$$

$$RT\rho\vec{u}(\vec{x},t) = \sum_{i=0}^{8} g_i(\vec{x},t)\vec{e}_i + \frac{RT\delta t}{2}(\vec{F}_s+\vec{G}) \tag{16}$$

$$p(\vec{x},t) = \sum_{i=0}^{8} g_i(\vec{x},t) - \frac{1}{2}\vec{u}(\vec{x},t)\cdot\vec{\nabla}\psi(\rho)\delta t. \tag{17}$$

3. Numerical simulations

We performed a series of numerical simulations using a parallel version of the LB model described above in order to study the effect of the applied body force G and the nw-phase fraction S_{nw} on the size distribution of the non-wetting blobs during the immiscible two-phase flow in 2D pore networks. The porous medium is represented by a 2D computational domain of size $L^2 = 1024^2\delta x^2$ that consists of randomly distributed solid and void square blocks of size $n^2 = 16^2\delta x^2$ (Fig. 1(a)). This produces a random pore network of solid and void blocks with a size of $N^2 = (1024/16)^2 = 64^2$. The probability of finding a void block at each one of the N^2 positions in the network is equal to ε, where ε is the porosity of the network. The probability of finding a solid block is $1-\varepsilon$. The pore network porosity is set at a very large value $\varepsilon = 0.729$ so that the 2D pore network is percolating (i.e. the void space is continuous in both directions).

Initially, we consider that the fluids (w-phase and nw-phase) also reside in blocks of size $n^2\delta x^2$ distributed at random replacing the void blocks with a probability S_w for the w-phase and $S_{nw} = 1-S_w$ for the nw-phase, where S_w is the area fraction of the w-phase (Fig. 1(b)). The pore network is subject to periodic boundary conditions in all directions. A constant body force G is applied along the x direction and the system is allowed to reach a "steady state" where the average values of the superficial velocities of the w- and nw-phases, and the number of nw-phase blobs, remain practically constant in time, although the temporal fluctuations may be significant. This typically requires more than $10^6\delta t$ depending on the value of the body force G. The kinematic viscosity of both phases is taken to be equal by applying the same relaxation time $\tau = 0.8$ for both phases.

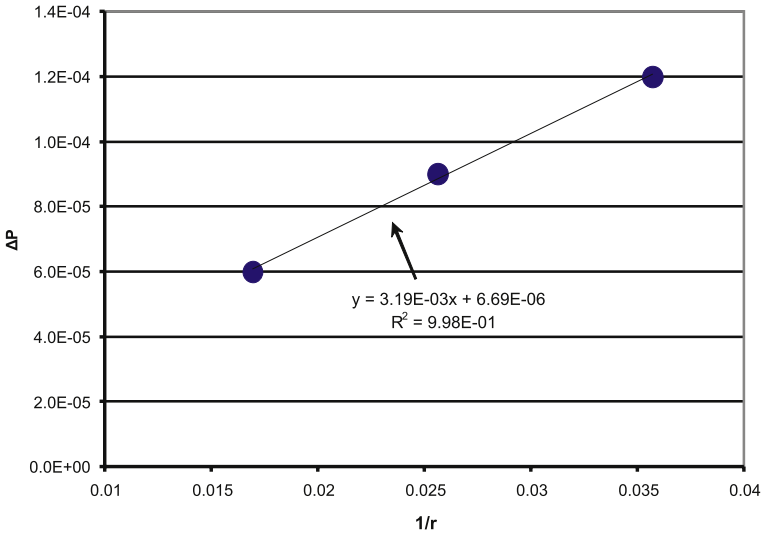

Fig. 2. Pressure drop across the interface of a circular non-wetting drop vs. the drop curvature $1/r$.

The selection of T_r for Eq. (9) can be arbitrary in the region $T_r < 1$. However, it has been shown in previous studies [15] that the model is more stable and captures phase separation more accurately for temperatures closer to the critical temperature. For this reason $T_r = 0.95$ is selected. The pressure and the density corresponding to the same chemical potential are calculated through Eq. (9) using Maxwell's equal area rule. Thus $p = 0.1068\rho_0\delta x^2/\delta t^2$, $\rho_{nw} = 0.5790\rho_0$ and $\rho_w = 1.4617\rho_0$, are found respectively. Here ρ_0 is a reference density which is set equal to unity.

However, the model can be applied for arbitrary pairs of density ρ^*_{nw} and ρ^*_w by interpolating over these two density values [14].

$$\rho^* = \rho^*_{nw} + \frac{\rho - \rho_{nw}}{\rho_w - \rho_{nw}}(\rho^*_w - \rho^*_{nw}). \tag{18}$$

In this case, the Maxwell equal area densities are used in Eqs. (2), (7), (13), (14) and (15) for mass conservation, while the rescaled densities ρ^*_{nw} and ρ^*_w are used in Eqs. (3), (8)–(12), (16) and (17) for momentum conservation and the calculation of interfacial forces [14]. In our simulations we take $\rho^*_{nw} = 1.0\rho_0$ and $\rho^*_w = 1.5\rho_0$. The density assigned to the solid sites is taken equal to the w-phase density, in order to produce a perfectly wet pore network [16].

The interfacial tension is implemented in the simulations by setting $a\sigma^2 = 0.15$ in lattice units. The surface tension produced for the selected density ratio can be easily calculated by applying Laplace's law for a stationary circular drop of the nw-fluid [17]. We consider a 2D computational domain of size $200^2\delta x^2$ with a circular drop of the nw-fluid located at the center. The radius of the drop is varied from $R = 20\delta x$ to $R = 60\delta x$ and the hydrodynamic pressure both inside and outside the drop are calculated using Eq. (17).

The pressure drop across the interface follows Laplace's Law:

$$p_{nw} - p_w = \frac{\gamma}{r}. \tag{19}$$

Fig. 2 shows the pressure drop across the interface of a stationary non-wetting drop with respect to the curvature $1/r$. The slope of the curve is equal to the surface tension $\gamma = 3.19 \cdot 10^{-3}\rho_0\delta x^3/\delta t^2$.

Alternatively, the surface tension can be calculated according the vdW theory where in the vicinity of the critical point, the EOS for the rescaled fluid densities can be simplified producing the following expression for the bulk free energy E_0 [18]:

$$E_0 = \beta(\rho^* - \rho^*_w)^2(\rho^* - \rho^*_{nw})^2. \tag{20}$$

The parameter β is related to the thickness of the interface ℓ through:

$$\beta = \frac{8a\sigma^2}{\ell^2(\rho^*_w - \rho^*_{nw})^2}. \tag{21}$$

The thickness of a planar interface can be related with the density profile by:

$$\rho^*(z) = \frac{\rho^*_w + \rho^*_{nw}}{2} + \frac{\rho^*_w - \rho^*_{nw}}{2}\tanh(2z/\ell). \tag{22}$$

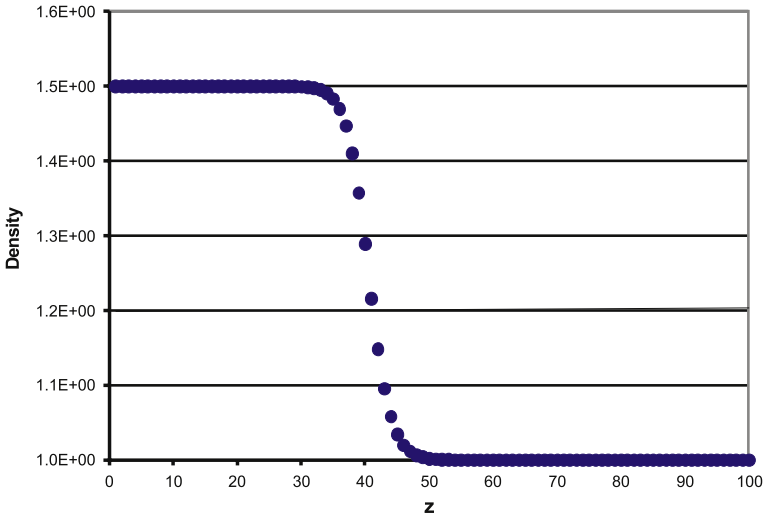

Fig. 3. Density profile across the fluid–fluid interface.

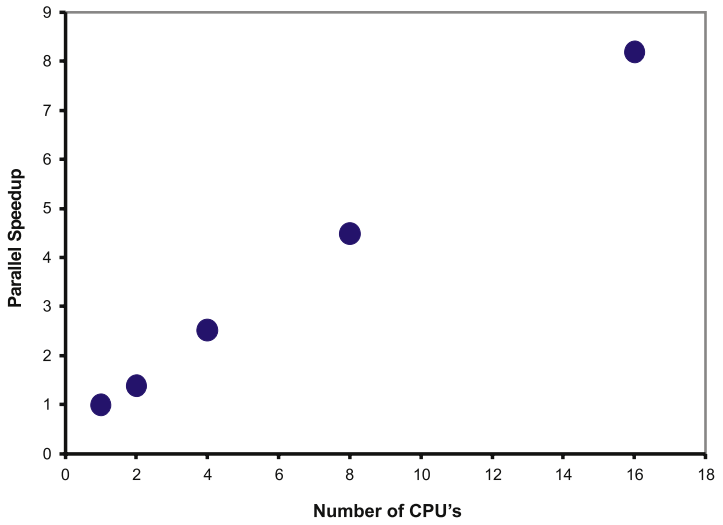

Fig. 4. Parallel speedup.

Plotting the density profile across the interface (Fig. 3), we find that $\ell = 7\delta x$ for $r = 60\delta x$, which after substitution in Eq. (21) yields $\beta = 0.09796$. The surface tension is then calculated by:

$$\gamma = \frac{(\rho_w^* - \rho_{nw}^*)^3}{6}\sqrt{2a\sigma^2\beta} \tag{23}$$

which gives $\gamma = 3.57 \cdot 10^{-3}\rho_0\delta x^3/\delta t^2$, in good agreement with the value obtained by Laplace's Law.

The Lattice-Boltzmann model described above is parallelized for implementation on distributed memory computers using the Message Passing Interface (MPI) libraries. The computational domain (2D) is decomposed in the y-direction in order to take advantage of Fortran's column-major storage of multi-dimensional array elements. This scheme ensures that array elements exchanged across processors with MPI are located in continuous memory blocks. The parallel speedup of our algorithm is shown in Fig. 4.

4. Results and discussion

4.1. Steady state flow conditions

The randomness and heterogeneity of the porous medium can result in the production of a distribution of nw-phase blobs of different sizes and shapes. The blobs flow through the porous medium under the combined effect of capillary and viscous forces. Capillary forces are proportional to the interfacial tension γ which is kept constant in our study.

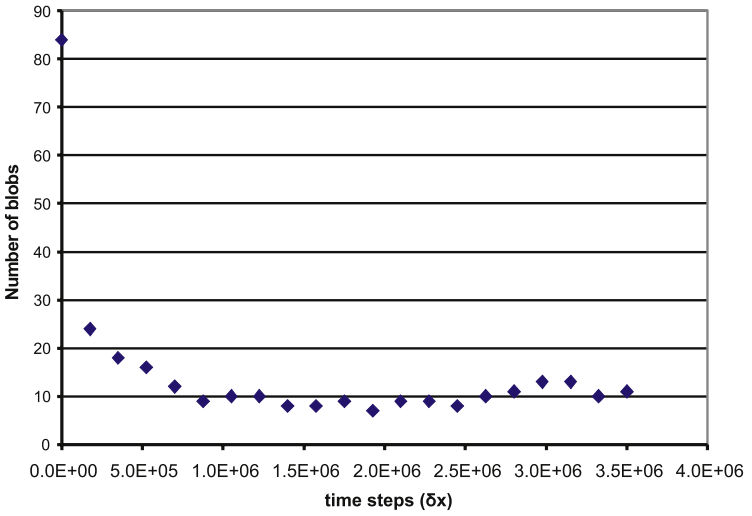

Fig. 5. Temporal evolution of blob numbers.

Viscous forces are proportional to the superficial velocity of the w-phase, u_w, which is produced under different values of G and S_w. The relative magnitude of these forces, expressed through the capillary number Ca, determines the rate at which blobs coalesce and the rate at which single blobs breakup into smaller ones. These forces also determine the ratio of the mobile blobs that flow through the pore space to the stranded blobs that are immobilized in low permeability regions of the porous medium.

The dynamic breakup occurs when larger nw-phase blobs flow through lower permeability regions of the pore network. The blobs deform under the combined effect of capillary and viscous forces in order to penetrate the smaller pore throats. At this stage, the frontal and rear parts of the blobs are subjected to different pressure gradients at each side of the pore throat and this causes further deformation and eventually breakup into two smaller blobs. This process is favored by relatively large values of the body force G (which corresponds to larger capillary numbers Ca) where the pressure gradients through the porous medium are more steep and viscous forces cause significant deformation of the interface of the blobs. Furthermore, larger blobs are expected to breakup at higher rates than smaller ones because they are subjected to larger pressure gradients as they move through narrow pore throats.

Coalescence occurs when two of more nw-phase blobs come in contact with each other as they flow through the porous domain. The interfacial tension forces smaller blobs to coalesce in order to produce a larger thermodynamically stable blob with a lower interfacial free energy. In certain cases of stranded blobs, coalescence is followed by the mobilization of stranded blobs as the larger ones are subject to larger pressure gradients. In general, blob coalescence is favored by larger values of the interfacial tension and thus smaller values of G and Ca.

All blobs, both mobile and stranded, undergo a continuous life-circle during which the continuously breakup into smaller blobs and coalesce with other to form larger ones. The system reaches a "steady state" condition after several million time steps δt where the rate of blob breakup becomes equal to the rate of coalescence and the number of blobs remains practically constant with time. Fig. 5 shows the temporal evolution of the nw-phase blobs in one typical simulation. In order to explore the uniqueness of the solution, we performed simulations starting from different initial numbers of blobs, keeping constant the area fraction of the nw-phase. In all cases the steady state solution was similar.

Fig. 6 shows the temporal evolution of both the wetting and non-wetting superficial velocities in one typical simulation. The superficial phase velocity is calculated by integrating the interstitial velocities of each phase divided by the overall domain area. The system reaches a steady state value where the average velocities remain practically constant with time although the temporal fluctuations are relatively large.

4.2. Effect of G and S_{nw}

As stated earlier, the numerical simulations are carried out until the superficial velocities and the numbers of the nw-phase blobs reach a steady state, where the average values remain practically constant. Both the superficial fluid velocities and the number of the nw-phase blobs at steady state conditions are determined by the applied body force G and the area fraction of the nw-phase S_{nw}.

The temporal evolution of the superficial velocities of the w- and nw-phase, when the w-phase fraction is $S_w = 0.9$, are shown in Fig. 7(a) and (b), respectively, for $G = 4 \cdot 10^{-6}\rho_0\delta x/\delta t^2$ and $G = 2 \cdot 10^{-5}\rho_0\delta x/\delta t^2$. The corresponding capillary numbers are $Ca = 0.015$ and $Ca = 0.085$, respectively. Larger values of G produce higher pressure gradients across the porous domain and larger values of the superficial velocities, as expected. The superficial w-phase velocity reaches a steady state value within a few thousand time steps and it remains practically constant from that point on. The w-phase velocity

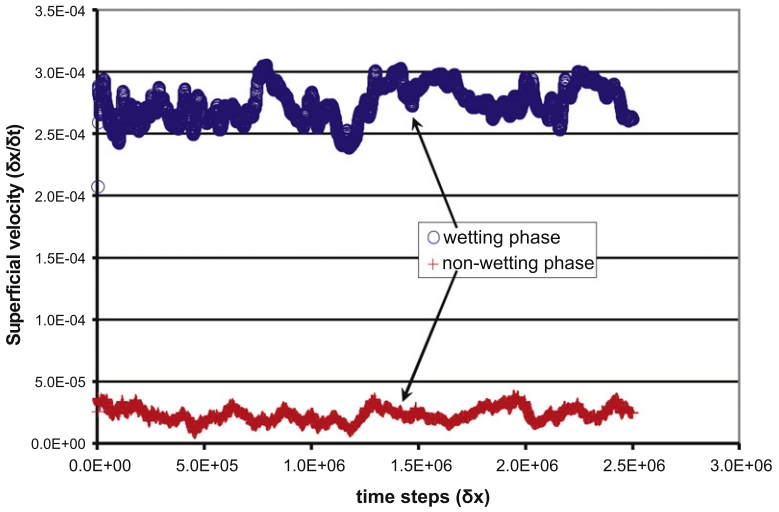

Fig. 6. Temporal evolution of superficial fluid velocities.

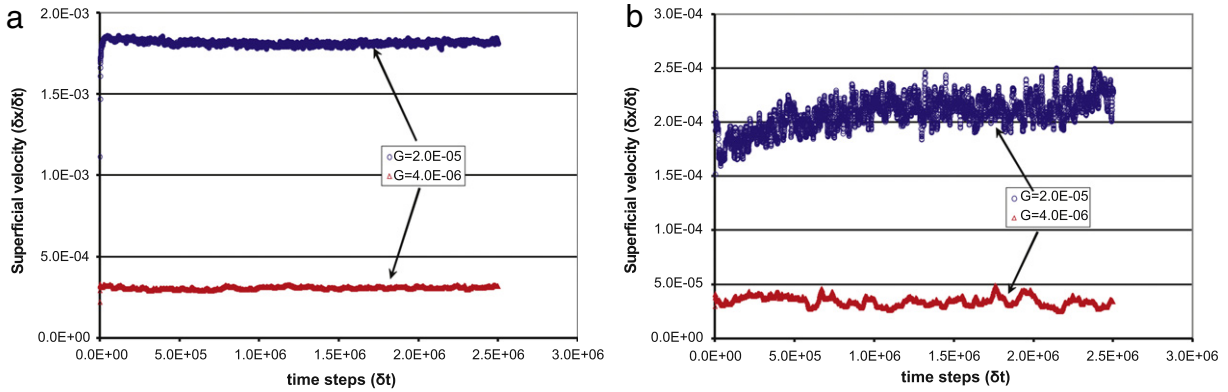

Fig. 7. Temporal evolution of wetting (a) and non-wetting (b) superficial fluid velocities for various values of G and $S_w = 0.9$.

and the resulting capillary number are directly proportional to the value of the body force G (Fig. 7(a)), which shows that for these values of G and S_w viscous forces dominate over capillary forces, as expected for this range of Ca [1]. The superficial nw-phase velocity (Fig. 7(b)) presents significant temporal fluctuations especially for larger values of G (and Ca). These fluctuations should be attributed to the pressure build-up in lower permeability regions of the pore network where the blobs coalesce and eventually breakup when the capillary pressure exceeds a critical value.

When the nw-phase fraction increases, the capillary forces on the nw-phase ganglia become more significant as shown in Fig. 8 for $S_w = 0.7$. The steady state superficial w-phase velocity is lower for all values of G (Fig. 8(a)) compared to the steady state velocities of the w-phase for the same values of G shown in Fig. 7(a) for $S_w = 0.9$. The capillary numbers are $Ca = 0.047$ for $G = 2 \cdot 10^{-5}\rho_0\delta x/\delta t^2$ and $Ca = 0.0067$ for $G = 4 \cdot 10^{-6}\rho_0\delta x/\delta t^2$, respectively. This should be attributed to the formation of larger nw-phase ganglia that block the low permeability flow paths and reduce significantly the relative permeability of the w-phase. Furthermore, for $S_w = 0.7$ the w-phase velocity is not directly proportional to G as for $S_w = 0.9$, but decreases at a faster rate as G decreases. As G decreases, capillary forces become more dominant over viscous forces, the rate of dynamic breakup decreases and the percentage of stranded nw-phase blobs also increases. It is also very interesting to note that for $S_w = 0.7$ the superficial velocities of the w- and nw-phase are practically equal (Fig. 8).

According to Dias and Payatakes [2], viscous forces dominate over capillary forces when the Capillary number is $Ca > 10^{-5}$, which is the case for all the simulation presented above. Under these conditions the effect of the viscosity ratio M is crucial. When $M > 1$, fluid/fluid interfaces become unstable along the direction of the flow and the blobs span across the domain producing viscous fingering patterns. The condition $M > 1$ favors the mobilization of stranded blobs and may produce relative permeabilities greater than one for the non-wetting phase [16]. In our simulations the viscous ratio is always $M = 2/3 < 1$ and fluid/fluid interfaces are stable. The effect of M will be studied in a forthcoming publication.

Fig. 9 shows the temporal evolution of the number of the nw-phase blobs for $S_w = 0.9$ and $S_w = 0.7$. The effect of G is more profound when the nw-phase area fraction is relatively low (Fig. 8(a)). The number of blobs increases with G because the dynamic breakup of the nw-phase blobs intensifies. Similar findings have been reported by [4] using a mechanistic pore

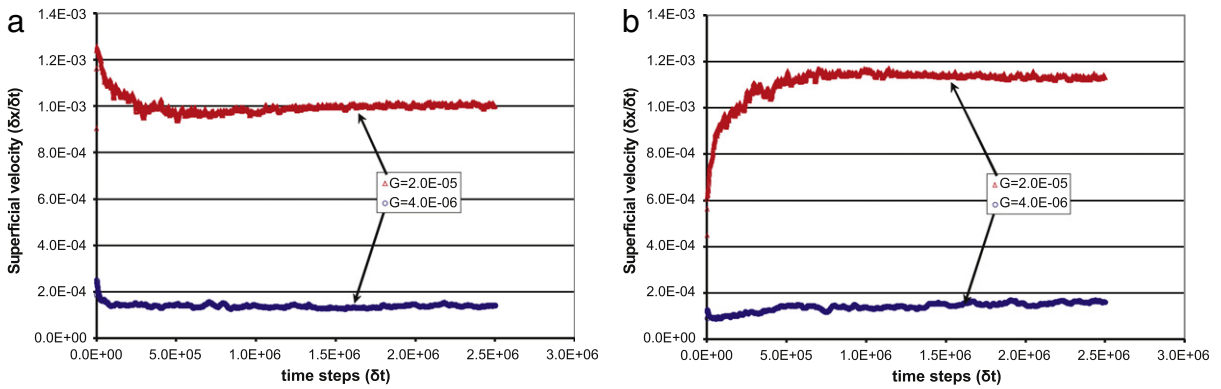

Fig. 8. Temporal evolution of wetting (a) and non-wetting (b) superficial fluid velocities for various values of G and $S_w = 0.7$.

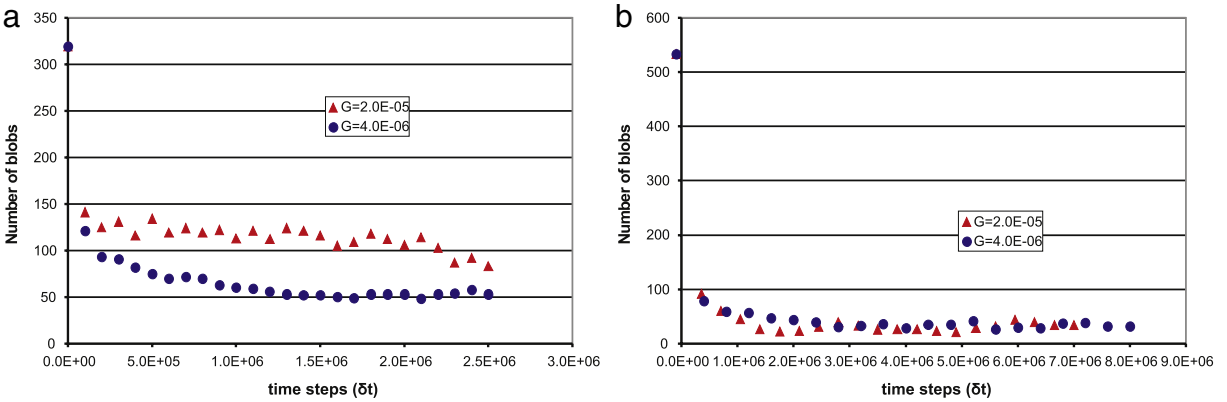

Fig. 9. Temporal evolution of the number of non-wetting blobs for various values of G for $S_w = 0.9$ (a) and $S_w = 0.7$ (b).

network model. As the nw-phase fraction increases, the effect of G becomes negligible because the porous medium is rich in nw-phase and the nw-phase blobs span the entire domain, including both low and high permeability regions, leaving little space for smaller blobs. Furthermore, for larger values of S_{nw}, the blobs become longer and the pressure gradient across it increases, resulting in a higher probability of mobilization. According to Amili and Yortsos [7], increasing the nw-phase fraction S_{nw}, produces a blob crowding effect which also results in a higher probability of mobilization and dynamic breakup as the flow path for the w-phase is restricted and viscous forces increase to match the applied pressure gradient. This is also observed in our simulations for $S_w = 0.7$, where the nw-phase flows mainly through a few spanning blobs (Fig. 10 for $S_w = 0.7$). The number of blobs remains practically constant regardless of G (Fig. 9(b)) although the blob size distribution changes.

Finally, we plot the phase distribution patterns at an arbitrary time step ($t = 2 \cdot 10^6 \delta t$) at "steady state" for all values of G and S_w presented in Fig. 10. This figure shows that for larger values of the applied body force G, the blobs become longer in shape, oriented in the direction of the flow and may even span the entire domain when the nw-phase fraction is sufficiently large (i.e. for $S_w = 0.7$). In this extreme case, the blobs coalesce into a few large spanning blobs providing a continuous nw-phase path along the entire porous medium. In the opposite case, when the nw-phase fraction is low, the number of the blobs increases as G increases, while their average size decreases.

5. Conclusions

We employed the Lattice-Boltzmann method for the simulation of immiscible two-phase flow through a 2D porous domain when the area fraction of the non-wetting phase is relatively low and it flows in the form of disconnected blobs. The forcing terms in the LB model used in this study are derived using a mean-field approach for the fluid density close to interfaces and the Gibbs–Duhem equation for chemical equilibrium. We studied the population dynamics of the non-wetting fluid blobs, namely the temporal evolution of the average blob size with respect to the applied body force and the wetting phase fraction. Our results show that the system reaches a "steady state" where the average values of dependent parameters, such as the superficial velocities of both phases, and the number and size distribution of the blobs remain practically constant in time, although the temporal fluctuations around average values may be significant. We show that the average volume of the blobs decreases (and the population of the blobs increases) as the body force increases, namely as

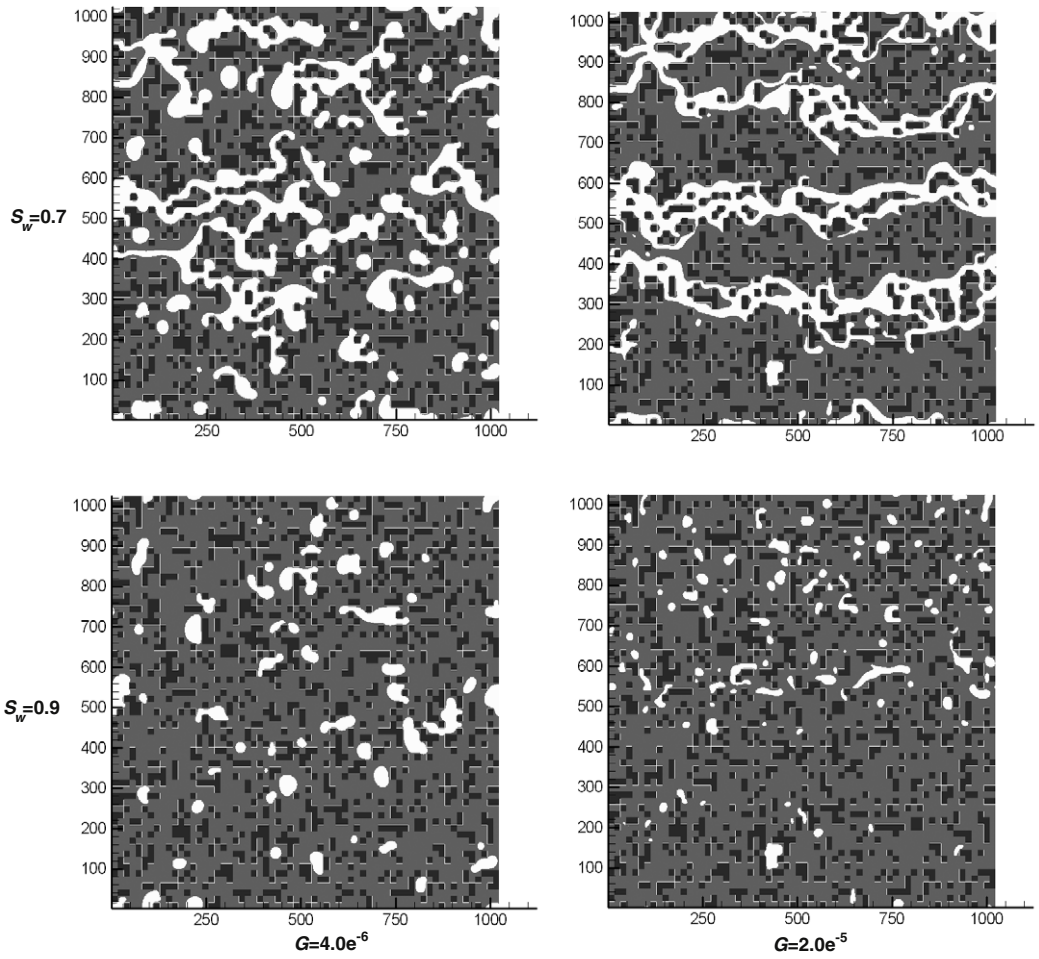

Fig. 10. Phase distribution patterns at an arbitrary time step ($t = 2 \cdot 10^6 \delta t$) for all values of G and S_w considered in this study.

the viscous forces become more significant over capillary forces because the dynamic breakup intensifies under these conditions. The effect of the wetting area fraction on the number of the blobs is more complex; as the wetting fraction decreases at constant body force, the blobs cover larger areas within the pore space producing larger pressure gradients and the dynamic breakup intensifies resulting in increasing blob numbers. However, below a critical value of the wetting area fraction where the non-wetting phase begins to span the entire pore network, the number of blobs begins to decrease, as smaller blobs coalesce to the larger spanning ganglion.

The numerical approach considered in this study has several advantages, including the straightforward treatment of complicated boundary structures and the significant parallel efficiency of the algorithm, but also several limitations, as with all numerical methods. Given the mesoscopic nature of the method, the computational resources required are significant. However, this is easily overcome due to the parallel efficiency of the method that allows for the solution of flow problems in very large 3D domains. This LB model is also known to have stability issues for large density and viscosity ratios. This is due to the discretization scheme which is used to track the fluid/fluid interfaces. Larger ratios lead to large density gradients and sharper interface profiles which are known sources for numerical instabilities. This problem has been addressed in the past using more efficient schemes for the calculation of density gradients.

References

[1] A.C. Payatakes, Dynamics of oil ganglia during immiscible displacement in water-wet porous media, Ann. Rev. Fluid Mech. 14 (1982) 365–393.
[2] M.M. Dias, A.C. Payatakes, Network models for two-phase flow in porous media. I: Immiscible microdisplacement of non-wetting fluids, J. Fluid Mech. 164 (1986) 305–336.
[3] M.M. Dias, A.C. Payatakes, Network models for two-phase flow in porous media. II: Motion of oil ganglia, J. Fluid Mech. 164 (1986) 337–358.
[4] G.N. Constantinides, A.C. Payatakes, Network simulation of steady-state 2-phase flow in consolidated porous-media, AIChE J. 42 (1996) 369–382.
[5] K.M. Ng, A.C. Payatakes, Stochastic simulation of the motion, breakup and stranding of oil ganglia in water-wet granular porous media during immiscible displacement, AIChE J. 26 (1980) 419–429.
[6] M.S. Valavanides, G.N. Constantinides, A.C. Payatakes, Mechanistic model of steady-state two-phase flow in porous media based on ganglion dynamics, Transp. Porous Med. 30 (1998) 267–299.

[7] P. Amili, Y.C. Yortsos, Darcian Dynamics: A New Approach to the Mobilization of a Trapped Phase in Porous Media, Transp. Porous Media 64 (2006) 25–49.
[8] S. Succi, The Lattice-Boltzmann Equation, Oxford University Press, New York, 2001.
[9] X. Shan, H. Chen, Lattice Boltzmann model for simulating flows with multiple phases and components, Phys. Rev. E 47 (1993) 1815–1819.
[10] X. Shan, H. Chen, Simulation of nonideal gases and liquid–gas phase transitions by the lattice Boltzmann equation, Phys. Rev. E 49 (1994) 2941–2948.
[11] X. He, G.D. Doolen, Thermodynamic foundations of kinetic theory and lattice boltzmann models for multiphase flows, J. Stat. Phys. 107 (2002) 309–328.
[12] M.R. Swift, W.R. Osborn, J.M. Yeomans, Lattice Boltzmann simulation of nonideal fluids, Phys. Rev. Lett. 75 (1995) 830–833.
[13] X. He, X. Shan, G.D. Doolen, Discrete Boltzmann equation model for nonideal gases, Phys. Rev. E 57 (1998) R13–R16.
[14] X. He, S. Chen, R. Zhang, A lattice Boltzmann scheme for incompressible multiphase flow and its application in simulation of Rayleigh–Taylor instability, J. Comput. Phys. 152 (1999) 642–663.
[15] E.S. Kikkinides, A.G. Yiotis, M.E. Kainourgiakis, A.K. Stubos, Thermodynamic consistency of liquid–gas lattice Boltzmann methods: Interfacial property issues, Phys. Rev. E 78 (2008) 036702.
[16] A.G. Yiotis, J. Psihogios, M. Kainourgiakis, A. Papaioannou, A.K. Stubos, A lattice Boltzmann study of viscous coupling effects in immiscible two-phase flow in porous media, Colloids Surf. A 300 (2007) 35–49.
[17] R. Zhang, X. He, S. Chen, Interface and surface tension in incompressible lattice-Boltzmann multiphase model, Comput. Phys. Comm. 129 (2000) 121–130.
[18] J.S. Rowlinson, B. Widom, Molecular Theory of Capillarity, Dover Publications, 2003.